Electronic Supplementary Material (ESI) for Inorganic Chemistry Frontiers.

Iron(II) Complexes of 4-Sulfanyl, 4-Sulfinyl and 4-Sulfonyl 2,6-Dipyrazolylpyridine Ligands. A Subtle Interplay between Spin-Crossover and Crystallographic Phase Changes

Laurence J. Kershaw Cook, Rafal Kulmaczewski and Malcolm A. Halcrow*

School of Chemistry, University of Leeds, Woodhouse Lane, Leeds, UK LS2 9JT.
E-mail: m.a.halcrow@leeds.ac.uk

Supporting Information

Definitions of the structural parameters discussed in the main paper.

Σ and Θ are defined as follows:

$$\Sigma = \sum_{i=1}^{12} \left| 90 - \beta_i \right| \qquad\qquad \Theta = \sum_{j=1}^{24} \left| 60 - \gamma_j \right|$$

where β_i are the twelve *cis*-N–Fe–N angles about the iron atom and γ_i are the 24 unique N–Fe–N angles measured on the projection of two triangular faces of the octahedron along their common pseudo-threefold axis (Scheme S1). Σ is a general measure of the deviation of a metal ion from an ideal octahedral geometry, while Θ more specifically indicates its distortion towards a trigonal prismatic structure. A perfectly octahedral complex gives $\Sigma = \Theta = 0$.[1]

Because the high-spin state of a complex has a much more plastic structure than the low-spin, this is reflected in Σ and Θ which are usually much larger in the high-spin state. The absolute values of these parameters depend on the metal/ligand combination in the compound under investigation, however.

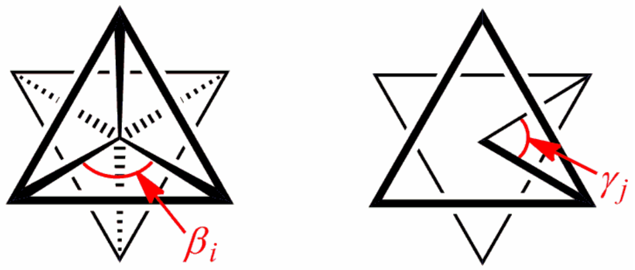

Scheme S1. Angles used in the definitions of the coordination distortion parameters Σ and Θ.

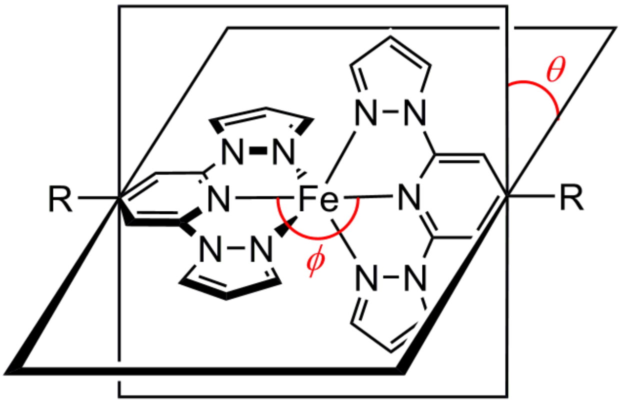

Scheme S2. Definition of the Jahn-Teller distortion parameters θ and ϕ.

These two parameters define the magnitude of an angular Jahn-Teller distortion, that is often observed in high-spin $[Fe(1\text{-}bpp)_2]^{2+}$ derivatives like **1** ($\theta \leq 90$º, $\phi \leq 180$ º).[2] Spin-crossover is inhibited if θ and ϕ deviate significantly from their ideal values, because the associated rearrangement to a more regular low-spin coordination geometry ($\theta \approx 90$º, $\phi \approx 180$º) cannot be accommodated by a rigid solid lattice.[3]

[1] P. Guionneau, M. Marchivie, G. Bravic, J.-F. Létard and D. Chasseau, *Top. Curr. Chem.*, 2004, **234**, 97.
[2] M. A. Halcrow, *Coord. Chem. Rev.*, 2009, **253**, 2493.
[3] M. A. Halcrow, *Chem. Soc. Rev.*, 2011, **40**, 4119.

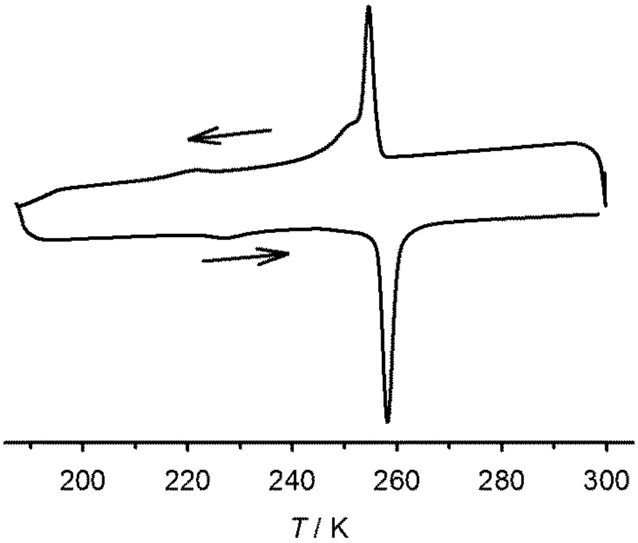

Figure S1. Differential scanning calorimetry (DSC) plot of a powder sample of $\mathbf{1[ClO_4]_2}$, at a scan rate of 5 $Kmin^{-1}$.

The main exotherm/endotherm centered around 256 K reproduces the features of the magnetic susceptiblity data, including the small hysteresis on the spin transition; and, the shoulder from the crystallographic phase change, that is observed in cooling mode but not in warming mode.

There is an additional weak hysteretic feature at around 225 K, that has no counterpart in the susceptibility data. One possible origin for this feature might be an anion order:disorder transition (all four unique ClO_4^- anion sites in the crystalline material are disordered at 240 K, but crystallographically ordered at 150 K).

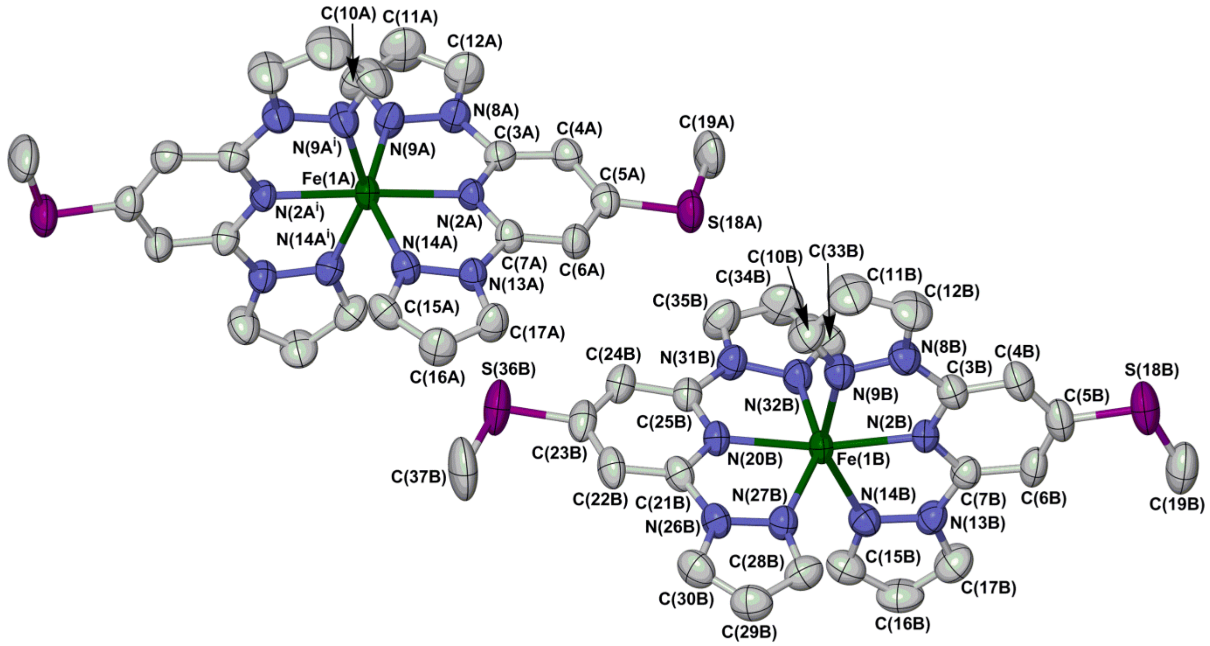

Figure S2. The two crystallographically unique $[\mathrm{Fe}(L^{\mathrm{SMe}})_2]^{2+}$ cations in phase 1 of $\mathbf{1[ClO_4]_2}$ at 280 K. Atomic displacement ellipsoids are at the 50 % probability level, and H atoms have been omitted for clarity. The view is the same as in Fig. 4 of the main article. Symmetry code: (i) 1–*x*, *y*, $^{3}/_{2}$–*z*.

Colour code: C, white; Fe, green; N, blue; S, purple.

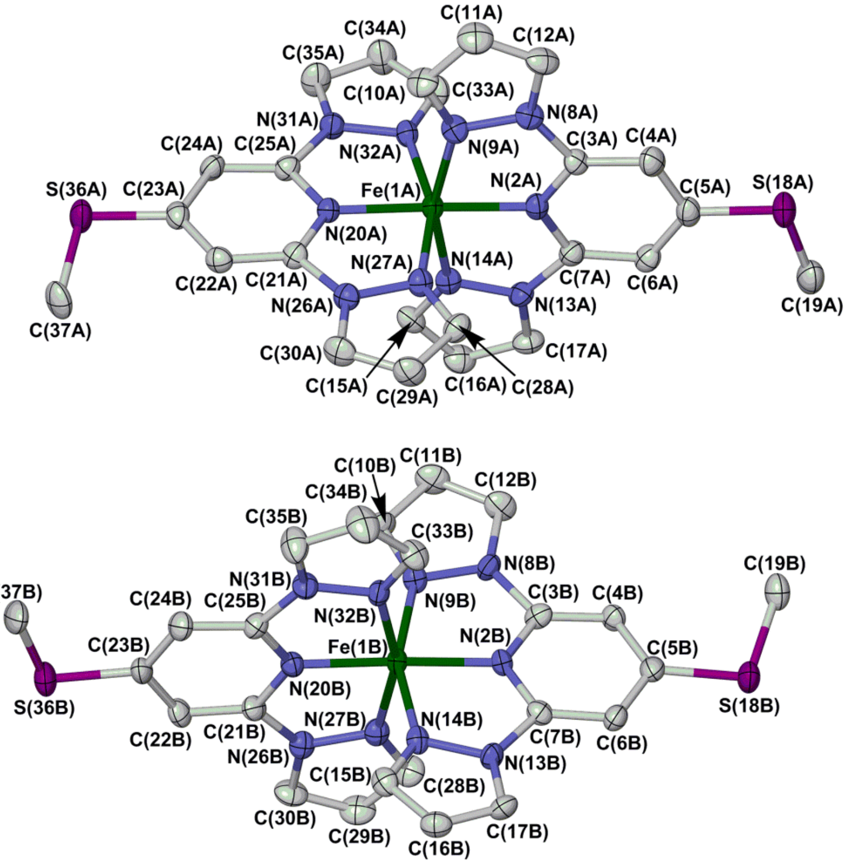

Figure S3. The two crystallographically unique $[\mathrm{Fe}(L^{\mathrm{SMe}})_2]^{2+}$ cations in phase 2 of $\mathbf{1[ClO_4]_2}$ at 150 K. Details as for Fig. S2.

Table S1. Intermolecular interactions in the crystal structures of **1[ClO$_4$]$_2$** – intra-layer *π*–*π* interactions between pyrazolyl rings (Fig. 5 of the main article).[a]

	Interplanar distance (Å)	Dihedral angle (°)	Lateral offset (Å)
T = 280 K (phase 1)			
[N(8A)-C(12A)]… [N(8A$^{\text{ii}}$)-C(12A$^{\text{ii}}$)]	3.55(3)	0	2.5
[N(8B)-C(12B)]… [N(31B$^{\text{iii}}$)-C(35B$^{\text{iii}}$)]	3.46(3)	5.5(5)	2.4
T = 253 K (phase 1)			
[N(8A)-C(12A)]… [N(8A$^{\text{ii}}$)-C(12A$^{\text{ii}}$)]	3.56(3)	0	2.3
[N(8B)-C(12B)]… [N(31B$^{\text{iii}}$)-C(35BA$^{\text{iii}}$)]	3.58(2)	4.1(5)	2.0
T = 240 K (phase 2)			
[N(8A)-C(12A)]… [N(26B$^{\text{iv}}$)-C(30B$^{\text{iv}}$)]	3.56(2)	7.4(5)	1.5
[N(26A)-C(30A)]… [N(8B)-C(12B)]	3.40(3)	9.4(5)	2.5
T = 150 K (phase 2)			
[N(8A)-C(12A)]… [N(26B$^{\text{iv}}$)-C(30B$^{\text{iv}}$)]	3.53(2)	7.8(4)	1.4
[N(26A)-C(30A)]… [N(8B)-C(12B)]	3.38(2)	9.3(4)	2.4

[a] Symmetry codes: (ii) 1–*x*, 2–*y*, 1–*z*; (iii) *x*, 1–*y*, $^{1}/_{2}$ +z; (iv) 1+*x*, *y*, *z*.

Table S2. Intermolecular interactions in the crystal structures of **1[ClO$_4$]$_2$** – inter-layer C–H…*π* contacts involving the methylsulfanyl groups (Fig. 5 of the main article). Only C…C contacts ≤3.6 Å are included, 0.1 shorter Å than the sum of the van der Waals radii of the interacting groups.[a]

	H…C (Å)	C…C(Å)	C–H…C (°)
T = 280 K (phase 1)			
None			
T = 253 K (phase 1)			
C(19A)–H(19B)…C(15B$^{\text{v}}$)	2.9	3.463(9)	115.4
T = 240 K (phase 2)			
C(19A)–H(19C)…C(30B$^{\text{vi}}$)	2.9	3.493(12)	117.1
C(37A)–H(37B)…C(16A$^{\text{vii}}$)	3.2	3.601(11)	109.0
C(37A)–H(37B)…C(11B$^{\text{vii}}$)	2.9	3.572(13)	128.5
C(19B)–H(19F)…C(12A$^{\text{viii}}$)	3.2	3.467(12)	99.9
C(19B)–H(19F)…C(16B$^{\text{ix}}$)	3.1	3.437(11)	104.8
T = 150 K (phase 2)			
C(19A)–H(19C)…C(30B$^{\text{vi}}$)	2.8	3.473(9)	122.6
C(37A)–H(37A)…C(16A$^{\text{vii}}$)	3.1	3.502(8)	107.7
C(37A)–H(37B)…C(11B$^{\text{vii}}$)	3.0	3.524(9)	114.8
C(19B)–H(19F)…C(12A$^{\text{viii}}$)	3.1	3.412(8)	102.5
C(19B)–H(19F)…C(16B$^{\text{ix}}$)	3.0	3.384(8)	104.0

[a] Symmetry codes: (v) *x*, 1+*y*, *z*; (vi) 1–*x*, $^{1}/_{2}$+*y*, $^{3}/_{2}$–*z*; (vii) 1–*x*, –$^{1}/_{2}$+*y*, $^{3}/_{2}$–*z*; (viii) –$^{1}/_{2}$+*x*, $^{3}/_{2}$–*y*, 1–*z*; (ix) $^{1}/_{2}$+*x*, $^{3}/_{2}$–*y*, 1–*z*.

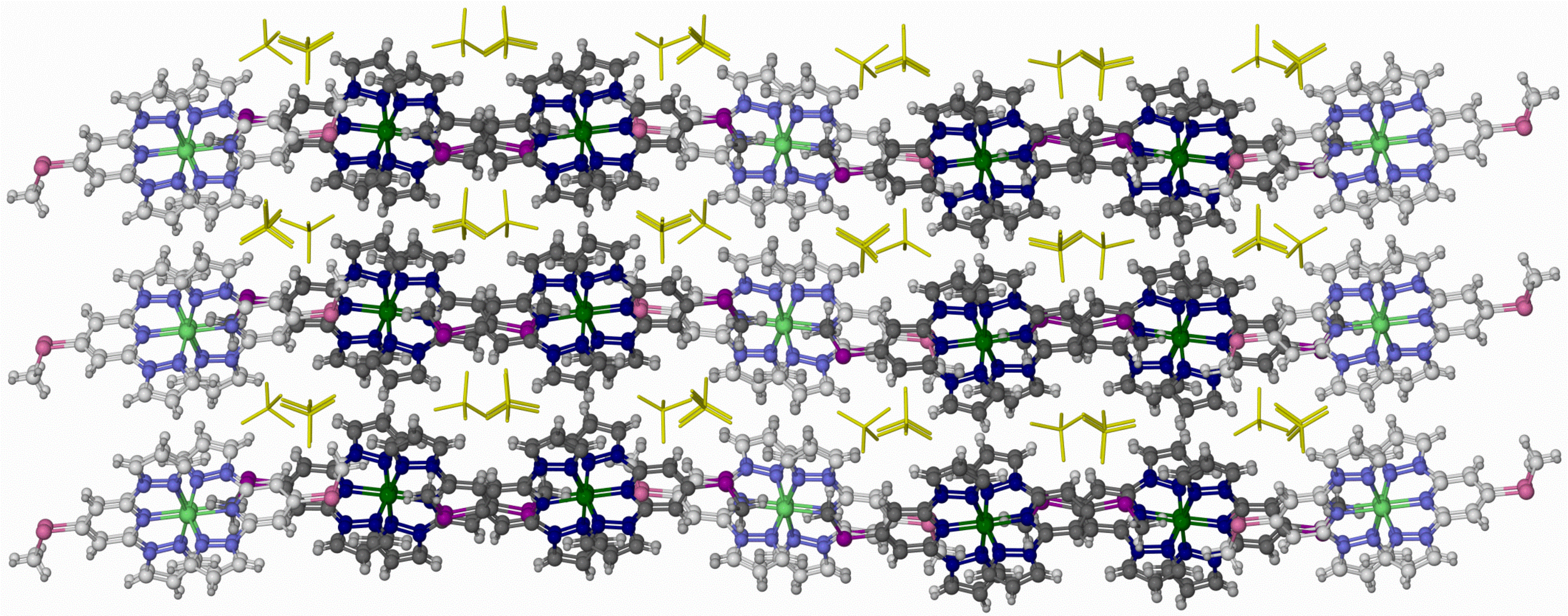

Figure S4 Packing diagram of phase 1 of **1[ClO$_4$]$_2$** at 253 K, showing the ABBABB stacking of the cation layers in the lattice. The 'A' cations have pale coloration while the 'B' cations are dark, and only one orientation of each disordered anion is shown. The view is approximately parallel to the [010] vector, with *a* horizontal. Colour code: C, white or dark gray; H, pale gray; Fe, green; N, blue; S, purple; ClO$_4^-$, yellow.

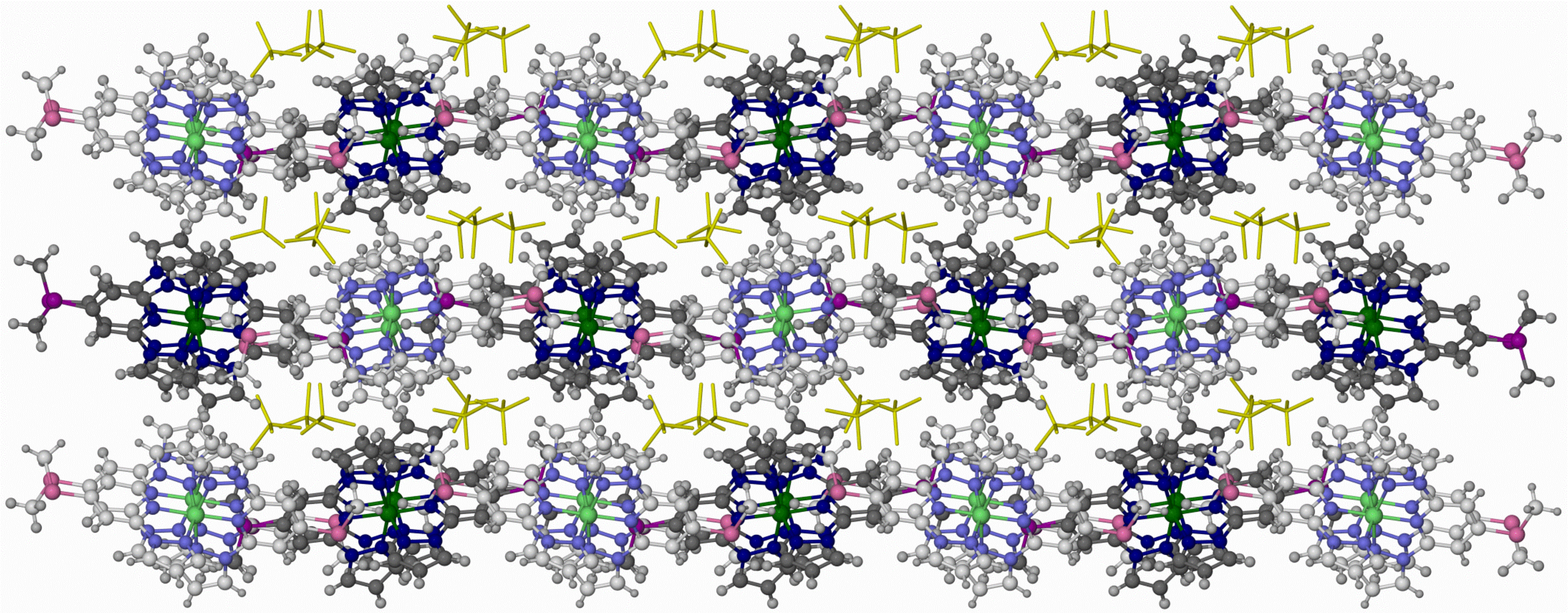

Figure S5 Packing diagram of phase 2 of **1[ClO$_4$]$_2$** at 240 K, showing the alternation of the crystallographic ‘A’ and ‘B’ cation sites within each cation layer. The ‘A’ cations have pale coloration while the ‘B’ cations are dark, and only one orientation of each disordered anion is shown. The view is parallel to the [001] vector, with *b* horizontal. Colour code: C, white or dark gray; H, pale gray; Fe, green; N, blue; S, purple; ClO_4^-, yellow.

Apart from a general realignment of the molecules, there are two important differences between phases 1 and 2:

- In contrast to phase 1, each cation layer in phase 2 is composed of alternating ‘A’ and ‘B’ crystallographic sites.

- In phase 1, the methylsulfanyl groups in each layer are all oriented the same way. In phase 2, the “up/down” or “left/right” methylsulfanyl orientations alternate between molecules within each layer.

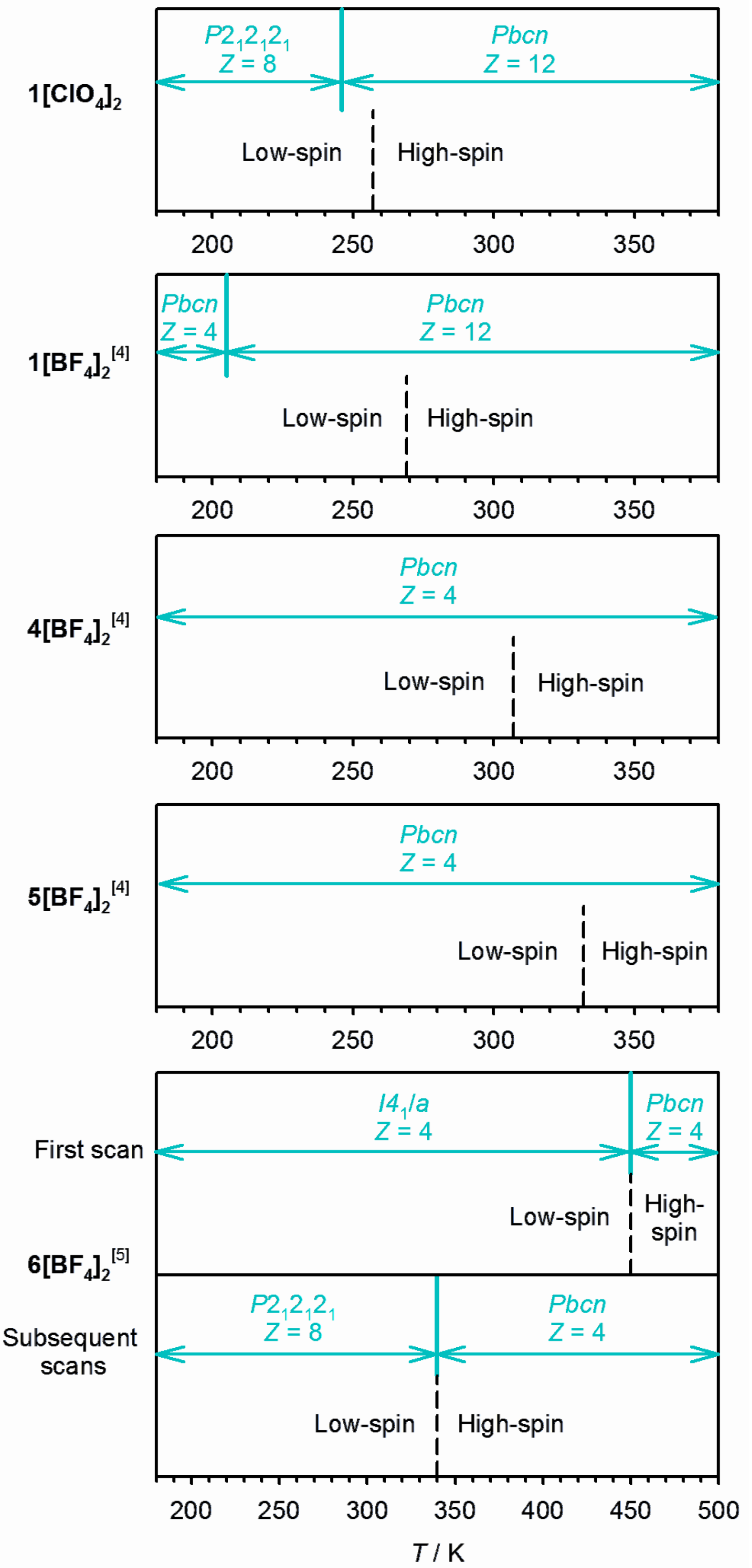

Figure S6 Summary of the spin-crossover temperatures (dashed black line) and the phase behaviour, including any phase transitions (solid cyan line) exhibited by a series of near-isostructural complexes that includes **1[ClO$_4$]$_2$**. See Scheme S1 for the structures of the literature compounds **4[BF$_4$]$_2$**-**6[BF$_4$]$_2$**.

The temperature scale for **6[BF$_4$]$_2$** is different from the other compounds in the Figure.

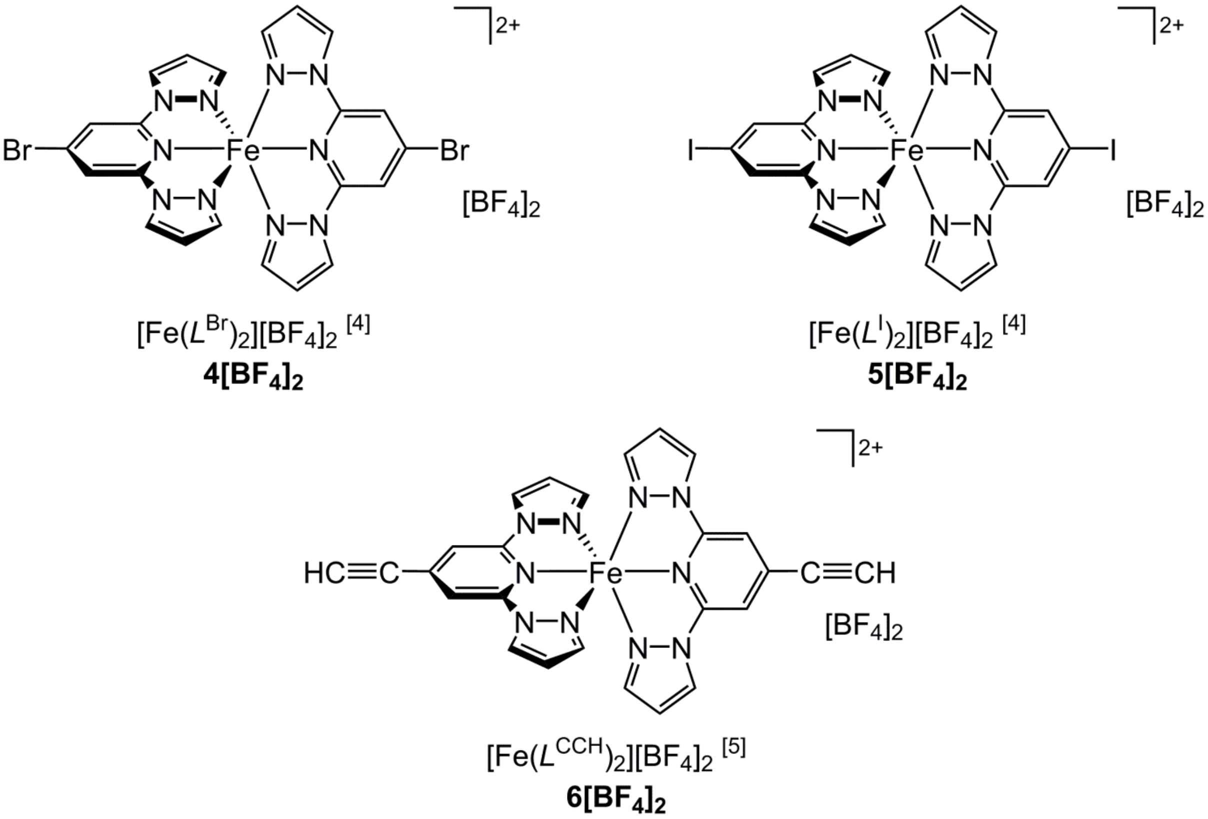

Scheme S3. Literature compounds referred to in Fig. S6.

[4] L. J. Kershaw Cook, H. J. Shepherd, T. P. Comyn, C. Baldé, O. Cespedes, G. Chastanet and M.A. Halcrow, *Chem. Eur. J.*, 2015, **21**, 4805.

[5] I. Šalitroš, O. Fuhr, A. Eichhöfer, R. Kruk, J. Pavlik, L. Dlháň, R. Boča and M. Ruben, *Dalton Trans.*, 2012, **41**, 5163.

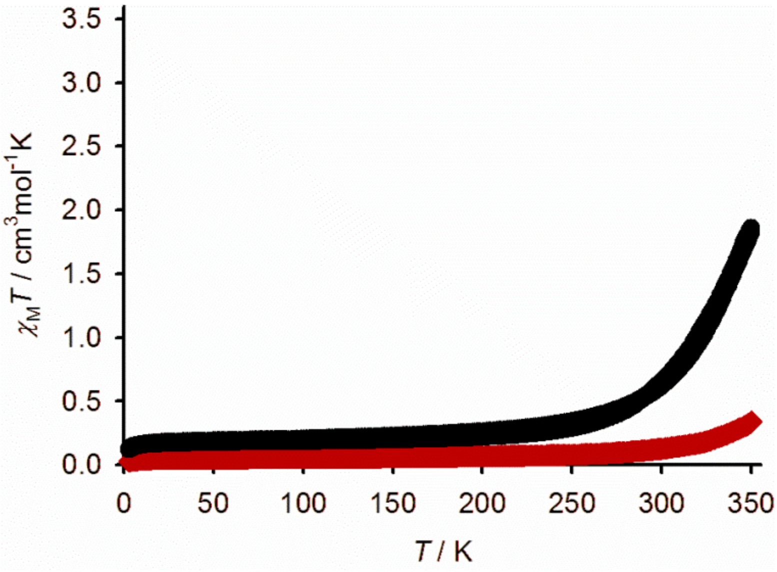

Figure S7 Variable temperature magnetic susceptibility data for **2[BF$_4$]$_2$** (black) and **3[BF$_4$]$_2$** (red) in the solid state, measured on a 300→5→350→300 K temperature cycle at a scan rate of 5 Kmin^{-1}.

The reversibility of the data for **2[BF$_4$]$_2$**·nH$_2$O upon heating and cooling shows that its spin-crossover is not associated with the loss of lattice water in the temperature range of the experiment.[6]

[6] See *e.g.*
a) M. Sorai, J. Ensling, R. M. Hasselbach and P. Gütlich, *Chem. Phys.*, 1977, **20**, 197;
b) K. H. Sugiyarto, D. C. Craig, A. D. Rae and H. A. Goodwin, *Aust. J. Chem.*, 1994, **47**, 869;
c) K. H. Sugiyarto, K. Weitzner, A. D. Rae and H. A. Goodwin, *Aust. J. Chem.*, 1997, **50**, 869;
d) M. Clemente-León, E. Coronado, M. C. Giménez-López and F. M. Romero, *Inorg. Chem.*, 2007, **46**, 11266;
e) T. D. Roberts, F. Tuna, T. L. Malkin, C. A. Kilner and M. A. Halcrow, *Chem. Sci.*, 2012, **3**, 349;
f) M. B. Bushuev, V. A. Daletsky, D. P. Pishchur, Y. V. Gatilov, I. V. Korolkov, E. B. Nikolaenkova and V. P. Krivopalov, *Dalton Trans.*, 2014, **43**, 3906.